

TWELFTH EUROPEAN ROTORCRAFT FORUM

Paper No. 57

AEROELASTIC STABILITY OF A BEARINGLESS CIRCULATION  
CONTROL ROTOR IN FORWARD FLIGHT

Inderjit Chopra

Professor

and

Chang-Ho Hong

Research Associate

September 22-25, 1986

Garmisch-Partenkirchen  
Federal Republic of Germany

Center for Rotorcraft Education and Research  
Department of Aerospace Engineering  
University of Maryland  
College Park, MD 20742, USA

# Aeroelastic Stability of a Bearingless Circulation Control Rotor in Forward Flight

Inderjit Chopra, Professor  
and  
Chang-Ho Hong, Research Associate

Center for Rotorcraft Education and Research  
Department of Aerospace Engineering  
University of Maryland, College Park, MD 20742, USA

## Abstract

The aeroelastic stability of flap bending, lag bending and torsion of a bearingless circulation control rotor blade in forward flight is examined using a finite element formulation. The flexbeam, the torque tube and the outboard blade are all discretized into beam elements, and the displacement compatibility conditions are introduced in assembled matrices. Quasisteady strip theory is used to evaluate aerodynamic forces, and the airfoil characteristics are taken from data tables. The effects of pneumodynamics and centrifugal pumping in the pressure duct are included to calculate jet momentum coefficient at a radial station. Two types of vehicle trim, propulsive and auxiliary power, are calculated from vehicle and rotor equilibrium equations through numerical integration of element forces in azimuth as well as in radial directions. The nonlinear periodic blade response is calculated using a finite element in time method in normal mode equations. The periodic linearized perturbation equations in modal space are analyzed for stability, using Floquet transition matrix theory. The effects of several parameters on blade stability are examined, including advance ratio, collective pitch, shaft tilt, propulsive and auxiliary power trim.

## Introduction

A circulation control rotor utilizes circulation control (CC) airfoils for the main rotor blade. A CC airfoil typically is of quasi-elliptic profile with thin jet of blowing taking place from a spanwise slot near the trailing edge (Fig. 1). Due to the Coanda effect, the air remains attached at the rounded trailing edge and the stagnation point shifts to the lower surface. With CC airfoils, lift can be controlled by geometric angle of incidence as well as the jet momentum. In a CC rotor, geometric pitch is held fixed, the cyclic control of lift is achieved through cyclic control of blowing. With a CC rotor, the hub design gets simplified and it is easy to implement high thrust at a reduced tip speed and a higher harmonic control system. The application of CC technology in the development of a full-scale rotor is currently being investigated. One concern is the dynamics of such rotors, influenced through CC aerodynamics.

The present paper will examine the aeroelastic stability of a bearingless CC rotor in forward flight.

A bearingless rotor is an example of a hingeless rotor where flap and lag hinges as well as pitch bearings are eliminated. One bearingless configuration which is analyzed in this paper is shown in Fig. 2. It consists of a single flexbeam and a wrap-around torque tube. There are two pitch-links for each blade, one located at the leading edge and the other at the trailing edge of the

torque tube. The pitch change of the blade is accomplished by rotating the torsionally stiff torque tube using pitch links, which in turn, twists the torsionally flexible flexbeam. This results in redundancy of load paths at the blade rotor, and therefore makes the analysis more involved than for hingeless or articulated rotors.

There has been only selected attempts to examine the aeroelastic stability of CC rotors. (See a recent review by Johnson<sup>2</sup>.) In Ref. 3, a basic formulation was developed to examine the stability of a CC rotor in hover. A simple blade model consisting of three degrees of motion: rigid flap, lag and feather rotations about hinges was used. Airfoil characteristics in the form of analytical expressions were used. It was shown that trailing edge blowing has substantial influence on blade stability. In Ref. 4, stability results were calculated for an elastic hingeless blade in hover using a finite-element formulation. The blade was assumed to undergo flap bending, lag bending and torsional deflections and airfoil characteristics from data tables were used. Again, it was confirmed that blowing has an important influence on blade dynamics. This finite element formulation was extended in Ref. 5 to examine the aeroelastic stability of bearingless rotors in hover.

In Ref. 6, the authors examined the aeroelastic stability of CC rotors in forward flight. The analysis was carried out for a simple blade model undergoing three degrees of motion (rigid flap, lag and feather angles.) Two types of trim procedures were used, propulsive and auxiliary power trim. Pneumodynamic effects were introduced in the calculation of aerodynamic forces on the blade. Nonlinear steady blade response was calculated using an iterative procedure based on Floquet theory, and stability of perturbation motion was determined using Floquet transition matrix theory. The blade response, as well as stability, were seen to be influenced by forward flight and was a function of several parameters including blowing level.

For bearingless rotors with conventional airfoils, there has been only limited research to examine their stability in forward flight. Recently, Dull<sup>7</sup> developed a finite element formulation to analyze the aeroelastic stability of different bearingless configurations in forward flight. The flexbeam, the torque tube and the outboard blade were discretized into beam elements, and the displacement compatibility and boundary conditions were satisfied. The nonlinear finite element (in space) equations were transformed to normal mode equations and these were then solved for steady response using a time finite element method. Stability results were calculated for an advanced bearingless configuration which included precone, blade twist, blade sweep, and a lag shear restraint. The calculated results were also correlated satisfactorily with measured data obtained from the stability testing of a model rotor in the wind tunnel.

In the present paper, the above finite element formulation<sup>7</sup> is modified to analyze the stability and response of a bearingless CC rotor in forward flight. The effects of several design parameters on blade stability are examined.

### Formulation

The blade is treated as an elastic beam and is assumed to undergo flap bending, lag bending, elastic twist and axial deflections. A finite element formulation based on Hamilton's principle is used. The flexbeam, the torque tube and the main outboard blade are discretized into beam elements, and each

element consists of fifteen degrees of freedom. Between elements there is a continuity of displacement and slope in flap and lag bending and continuity of displacement in elastic twist and extension. There are two internal nodes for extension and one for twist. The derivation of stiffness and inertial element properties are available in Ref. 8.

During the assembly of elements, the displacement compatibility conditions at the junction, where torque tube, flexbeam and main blade join, are introduced. The flexbeam is cantilevered at the root, whereas for the torque tube end there are no constraints on displacements except for a spring restraint in the pitch link direction. The necessary modifications needed in the assembled matrices due to compatibility and boundary conditions are shown in Ref. 5.

Quasisteady strip theory is used to obtain aerodynamic forces on the blade. The section lift, drag, and moment about the mid-chord (per unit span) are

$$\begin{aligned} L &= \frac{1}{2} \rho V^2 c c_l(\alpha, C_\mu) \\ D &= \frac{1}{2} \rho V^2 c c_d(\alpha, C_\mu) \\ M_{.5} &= \frac{1}{2} \rho V^2 c c_{m_{.5}}(\alpha, C_\mu) \end{aligned} \quad (1)$$

The aerodynamic coefficients  $C_l$ ,  $C_d$  and  $C_{m_{.5}}$  are taken from data tables.

The values of these coefficients depend on the airfoil geometry, including slot height, and are also a function of angle of attack  $\alpha$ , blowing momentum coefficient  $C_\mu$ , and local Mach number. In the present paper, the effects of

compressibility are neglected. The  $C_\mu$  is defined as

$$C_\mu = \frac{\dot{m}V_j}{qc} \quad (2)$$

where  $\dot{m}V_j$  is the jet momentum,  $q(=\frac{1}{2} \rho V^2)$  is the dynamic pressure, and  $c$  is the blade chord.

Between the duct pressure at the blade root (pneumatic valving system) and a radial station, there is a loss due to duct friction, a phase lag due to length, and a pressure<sup>9</sup> ram due to the centrifugal pumping. This phenomenon is called pneumodynamics<sup>9</sup>. The duct pressure at a radial station is obtained as

$$\begin{aligned} P_d &= (P_{dr} - P_\infty) \left\{ 1 - \eta_{duct} \left[ \frac{r}{R} - \left( \frac{r}{R} \right)_{root} \right] \right\} \\ &+ (P_{dr}/P_\infty) \frac{\rho}{2} \left( \frac{r}{R} V_{tip} \right)^2 \eta_{pump} \end{aligned} \quad (3)$$

and

$$P_{dr} = P_0 + P_{1c} \cos(\psi - \phi) + P_{1s} \sin(\psi - \phi)$$

where  $\phi$  is the phase lag for the pressure pulse at a radial station defined as

$$\phi = \frac{6 \text{ RPM}}{a_{\text{duct}}} (r - r_{\text{root}}) \text{ deg.} \quad (4)$$

where  $\eta_{\text{duct}}$  and  $\eta_{\text{pump}}$  are respectively centrifugal pump efficiency and duct friction loss coefficient. The  $V_{\text{tip}}$  is tip speed ( $\Omega R$ ),  $r_{\text{root}}$  is root radius (where the pressure duct starts),  $P_\infty$  is atmospheric pressure (1827 lb/ft<sup>2</sup>) and  $a_{\text{duct}}$  is speed of sound in duct (1274 ft/sec).

Once the duct pressure  $P_d$  at a radial station is known, then the blowing momentum can be calculated.<sup>10</sup> For example, with an incompressible flow condition in the jet nozzle, isentropic expansion relationship can be used to calculate  $C_\mu$ ,

$$C_\mu = 2 \frac{h}{c} \frac{1}{q} (P_d - P_\infty) \quad (5)$$

where  $h/c$  is slot height-to-chord ratio (typically .002), and  $P_d - P_\infty$  is duct gage pressure. The dynamic pressure at a radial station is

$$q = \frac{1}{2} \rho (\Omega R)^2 \left( \frac{r}{R} + \mu \sin \psi \right)^2 \quad (6)$$

In general, the flow conditions in the nozzle are compressible. For an unchoked subsonic jet,

$$C_\mu = 2 \frac{h}{c} (M_j / M_\infty)^2 \quad (M_j < 1) \quad (7)$$

where  $M_j$  is the jet Mach number and  $M_\infty$  is free-stream Mach number. The choked flow in the nozzle occurs when  $P_d / P_\infty$  is larger than 1.892. Then  $C_\mu$  is calculated as

$$C_\mu = \frac{2 \frac{h}{c} \frac{P_d}{P_\infty} M_j \left( \frac{2}{\gamma+1} \right)^{\frac{\gamma+1}{2(\gamma-1)}}}{M_\infty^2 \sqrt{1 + \frac{\gamma-1}{2} M_j^2}} \quad (8)$$

The jet Mach number for both choked and unchoked flows is calculated in terms of duct pressure

$$M_j = \sqrt{5 \left[ \left( \frac{P_d}{P_\infty} \right)^{\frac{\gamma-1}{\gamma}} - 1 \right]} \quad (9)$$

The above equations show that the blowing momentum coefficient is a function of radial position  $r$  and azimuth angle  $\psi$ .

For steady inflow in forward flight, a linear distribution model is used.

For our results, Drees<sup>11</sup> model is used.

The solution procedure consists of three phases: vehicle trim, steady blade response and stability of perturbation motion.

### Vehicle Trim

The trim solution calculates rotor controls and vehicle orientation for prescribed flight conditions. Two types of trim procedures are used, propulsive trim and auxiliary power trim.

The propulsive trim simulates the free flight condition. It is calculated from vehicle equilibrium equations, three forces (vertical, horizontal and lateral) and two moments (pitch and roll) equations. For specified weight coefficient  $C_w$ , collective pitch  $\theta_0$ , forward speed  $u$ , and cg positions  $x_{CG}$  and  $y_{CG}$  the solution calculates blowing settings ( $P_0, P_{1C}$  and  $P_{1S}$ ), steady rotor response ( $\beta_0, \beta_{1C}, \beta_{1S}$ ), vehicle orientation ( $\alpha_s$  and  $\phi_s$ ) and steady inflow  $\lambda$ . For trim calculations, only rigid flap response is used. The rotor forces are obtained by integrating numerically the elemental forces. The vehicle nonlinear equilibrium equations are solved iteratively using the Newton-Raphson method.

The auxiliary power trim is a constrained trim where part of the propulsive force is achieved through an auxiliary power source. For this trim, the vehicle orientation is prescribed and the solution is calculated from the vehicle vertical force equilibrium equation. For a specified weight coefficient  $C_w$ , collective pitch  $\theta_0$ , and advance ratio  $\mu$ , the trim solution calculates blowing settings ( $P_0, P_{1C}$ , and  $P_{1S}$ ) and rotor response ( $\beta_0, \beta_{1C}$  and  $\beta_{1S}$ ). Again, the solution procedure is similar to that used for propulsive trim. (For details, see Ref. 6)

### Blade Steady Response

The analysis calculates the steady deflected position of the blade along the azimuth for one complete cycle. The assembled finite element equations are nonlinear and periodic in nature. To reduce computation time, these large

number of finite element equations are transformed into a few normal mode equations using coupled vibration modes about the undeflected blade position. To include the effect of rigid body modes in torsional response, these vibration modes are calculated by freeing the twist degree at the torque tube end. (Ref.7)

The nonlinear normal mode response equations are solved for steady response using a finite element in time method based on Hamilton's principle in weak form. One cycle of time is divided into a number of azimuthal elements and then the periodicity condition is used to join the first and last elements. The assembly results in a set of nonlinear algebraic equations which are solved using the Newton-Raphson technique. (For details, see Ref. 13)

### Stability of Perturbation Motion

The perturbation motion of blade about its steady deflected position is linearized and examined for stability. For perturbation motion, the effects of unsteady aerodynamics are introduced approximately through a dynamic inflow model. A linear variation of perturbed inflow is assumed and the inflow components are related to rotor perturbation aerodynamic forces and moments.<sup>14</sup>

The blade finite element perturbation equations are transformed to modal space using coupled vibration modes about mean deflected position of the blade. These normal mode blade equations in the rotating frame are then transformed to the fixed frame using a multiblade coordinate transformation. These, in conjunction with the dynamic inflow equation, are then analyzed for stability using Floquet transition matrix theory. (For details, see Ref.15)

## Results and Discussion

Numerical results are calculated for a bearingless blade, consisting of a single flexbeam with wrap-around torque tube (Fig.2). The rotor characteristics are: Lock number  $\gamma = 7.2$ , solidity ratio  $C_w/\sigma = .13$ , four bladed, and zero precone. The chordwise offsets of the center of mass and the reference aerodynamic center from the elastic axis are considered to be zero, and the elastic axis is assumed to be at the midchord position. For airfoil characteristics, tabular data of a typical CC airfoil with trailing edge blowing is used. For stability calculations the structural damping for all modes is assumed to be zero. The other vehicle and rotor properties are given in Table 1. The nondimensional structural blade properties for different blade elements are given in Table 2.

### Propulsive Trim

Numerical results are calculated for  $C_w/\sigma = .1$ . Figures 3 (a) and 3 (b) show the vehicle propulsive trim solution for a collective pitch of zero. The propulsive trim parameters  $p_0$ ,  $P_{1c}$ ,  $P_{1s}$ ,  $\alpha_s$ ,  $\phi_s$  and  $\lambda$  are plotted for different forward speeds (in terms of advance ratio  $\mu$ ). An advance ratio of .5 represents a forward speed of about 250 ft/sec and a maximum tip speed of 750 ft/sec. The root blowing pressures, collective ( $P_0$ ) and cyclic ( $P_{1c}$  and  $P_{1s}$ ), are presented in terms of atmospheric pressure ( $P_\infty$ ). The flap angles ( $\beta_0, \beta_{1c}$  and  $\beta_{1s}$ ) are negligible for this highly stiff rotor and hence are not presented.

The trim solution is calculated iteratively from nonlinear equilibrium equations. As a conventional rotor, the shaft has to tilt more forward at larger  $\mu$  in order to compensate for the increasing parasite drag. The inflow  $\lambda$  first decreases and then increases with forward speed due to the combined effect of decreasing induced velocity and increasing disk tilt  $\phi_s$ . The collective and cyclic blowing pressure requirements with advance ratio  $S_\mu$  appear quite similar to the respective geometric pitch requirements of a conventional rotor (Panda and Chopra<sup>15</sup>). The cyclic blowing pressures ( $P_{1c}$  and  $P_{1s}$ ) are much smaller than the collective blowing pressure ( $P_0$ ). The periodic variation of dynamic pressure due to forward speed is compensated for by the cyclic blowing components. At low forward speeds, both  $P_{1c}$  and  $P_{1s}$  are of equal importance because of the uniform induced velocity; however at higher speeds,  $P_{1s}$  becomes larger than  $P_{1c}$ .

Figure 4 presents the time-dependent blade tip deflections for one complete cycle. The blade is set at zero collective pitch, and the propulsive trim solution is employed. These results are obtained by solving the nonlinear periodic equations iteratively using finite element method in time domain. For the numerical calculation, six equally spaced time elements per cycle ( $\Delta\psi = 60$  degrees) are used. The blade is extremely stiff in the flap mode (flap frequency = 2.3/rev) and, therefore a small flap deflection is expected. At a low forward speed ( $\mu = .2$ ), there is a little flap deflection. However, at high forward speeds, the flap deflection becomes greater induced by a larger variation in aerodynamic environment along the azimuth. At  $\mu = .4$ , the flap deflection consists primarily of the second harmonic with a maximum peak-to-peak amplitude of about 2 degrees, which is perhaps a large flap deflection for this highly stiff rotor.

Figure 5 shows the damping of the low frequency cyclic lag mode for different advance ratios and collective pitch. Results are obtained from the eigen solution of Floquet transition matrix. For the stability solution, 180 time steps per cycle ( $\Delta\psi = 2$  degrees) are used for numerical integration. The eigenvalues represent rotor modes in the fixed reference frame. For this case, the low frequency lag mode is a regressive mode. The damping is represented in terms of the real part of the complex eigen value,  $\alpha_\zeta$ . Note that  $\alpha_\zeta = \zeta_L \omega_\zeta$ , where  $\zeta_L$  is the viscous damping ratio of the lag mode, and  $\omega_\zeta$  is the frequency of lag mode nondimensional with respect to rotational speed. For the case of zero collective pitch, the damping level in lag damping is quite low in hover and stays that way even at high forward speeds. However, the inclusion of structural damping will increase the blade stability. In contrast, the negative collective pitch has a considerable stabilizing influence on the lag mode. The lag mode is unstable in hover and becomes stable at a moderate forward speed ( $\mu > .1$ ).

### Auxiliary Power Trim

Constrained trim calculates the rotor controls to achieve a desired thrust and shaft orientation. This type of trim condition is possible through an auxiliary propulsive device. With the auxiliary propulsive device, it is possible to achieve high forward speeds without causing excessive shaft tilts. Thus, the

subsequent results using constrained trim include a larger range of advance ratios (up to 1.0). An advance ratio of 1.0 represents a forward speed of about 500 ft/sec and a maximum tip speed of 1000 ft/sec. The compressibility effects, however, have not been considered in the present work.

The auxiliary power trim solution for -5 degree collective pitch and -5 degree shaft angle is shown in figure 6. The collective and cyclic components of blowing pressure at the blade root are quite similar to those obtained with propulsive trim for zero collective pitch. The collective pressure  $P_0$  is somewhat smaller at higher advance ratio because of reduced inflow through the rotor disk. For  $\mu = .84$ , the solution is not practical because of the pressure constraint ( $P_{\text{root}} < P_{\infty}$ ).

Figure 7 presents the flap deflection at the blade tip for one complete cycle. For this case, the rotor is set at zero shaft angle and -5 degrees collective pitch. For a low advance ratio ( $\mu = .2$ ), the flap deflection amplitude is small. At high advance ratio, there is considerable flap deflection, consisting primarily of a 2/rev component. For  $\mu = .5$ , the peak-to-peak amplitude is about 2.3 degrees, whereas, for  $\mu = 1.0$ , the peak-to-peak amplitude is about 5.7 degrees.

Figure 8 shows the lag mode stability results for shaft angle zero and -5 degrees. The collective pitch is set at -5 degrees for both cases. In both cases, the low frequency lag mode is unstable in hover and becomes stable at a very small forward speed ( $\mu > .04$ ). For the negative shaft angle, the lag mode is slightly more damped than that of the zero shaft angle case but becomes less damped at a higher forward speed ( $\mu > .25$ ). In fact, for  $\mu > .8$ , the lag mode for negative shaft tilt appears tending towards instability. The negative shaft is a rearward tilt of the rotor shaft, and the inflow through the rotor disk decreases, resulting in a decreased collective pressure requirement.

### Conclusions

A finite element formulation both in spatial coordinates and time has been applied successfully to calculate the stability and response of a bearingless rotor blade in forward flight. Results are obtained using propulsive trim as well as auxiliary power trim. Based on the results of this study, the following conclusions are drawn.

#### Propulsive Trim

- 1) Cyclic pressure requirements to trim a CC rotor are quite similar to the cyclic pitch requirements of a conventional rotor.
- 2) Flap deflection consists of 2/rev, and its amplitude increases with  $\mu$ . For example, for propulsive trim, the peak-to-peak amplitude at  $\mu = .4$  is 2 degrees, and for auxiliary power trim, peak-to-peak amplitude at  $\mu = 1.0$  is 5.7 degrees.

- 3) For propulsive trim with zero collective pitch, the lag mode is moderately stable and stays that way with forward speed. With a collective pitch of -10 degrees, the lag mode is unstable in hover and becomes stable at a moderate forward speed ( $\mu > .1$ ). The lag mode stability results with auxiliary power trim are quite similar to those for propulsive trim.
- 4) With negative shaft tilt (rearward), the lag mode becomes less stable at high forward speeds.

#### References

1. Linden, A.W. and Biggers, J.C.      X-Wing Potential for Navy Applications, 41st Annual Forum of American Helicopter Society, Fort Worth, Texas, May 1985.
2. Johnson, W.      Recent Developments in the Dynamics of Advanced Rotor Systems, NASA TM 86669, March 1985.
3. Chopra, I. and Johnson, W.      Flap-lag-torsion Aeroelastic Stability of Circulation - Controlled Rotors in Hover, Journal of the American Helicopter Society, Vol. 24, No. 2, April 1979, pp. 37-46.
4. Chopra, I.      Aeroelastic Stability of an Elastic Circulation Control Rotor Blade in Hover, Vertica, Vol. 8, No. 4, Oct. 1984, pp.353-371.
5. Chopra, I.      Aeroelastic Stability of a Bearingless Circulation Control Rotor Blade in Hover, Journal of the American Helicopter Society, Vol.30, No.4, Oct. 1985, pp. 40-47.
6. Chopra, I. and Hong, C.H.      Flap-lag-torsion Aeroelastic Stability of a Circulation Control Rotor in Forward Flight, Presented at Circulation Control Workshop, NASA Ames Research Center, Feb. 1986.
7. Dull, A.,      Aeroelastic Stability of Bearingless Rotors in Forward Flight, Ph.D Thesis, Department of Aerospace Engineering, University of Maryland, August 1986.
8. Sivaneri, N.T. and Chopra, I.      Finite Element Analysis for Bearingless Rotor Blade Aeroelasticity, Journal of the American Helicopter Society, Vol. 29, No.2, April 1984, pp.42-51.

9. Watkins, C.B., Reader, K.R.  
and Dutta, S.K.                      Pneumodynamic Characteristics of a  
Circulation Control Rotor Model,  
Journal of the American Helicopter  
Society, Vol. 30, No. 3, July 1985,  
pp.23-31.
  
10. Rogers, E.O., Schwartz, A.W.  
and Abramson, J.S.                    Applied Aerodynamics of Circulation  
Control Airfoils and Rotors, 41st  
Annual Forum of the American Helicopter  
Society, Fort Worth, Texas, May 1985.
  
11. Johnston, W.                        Helicopter Theory, Princeton University  
Press, Princeton, New Jersey, 1980.
  
12. White, F. and Blake B.B.            Improved Method of Predicting Helicopter  
Control Response and Gust Sensitivity,  
Presented at 35th Annual Forum of  
American Helicopter Society, Washington  
DC, May 1979.
  
13. Panda, B. and Chopra, I.            Dynamics of Composite Rotor Blades in  
Forward Flight with Application of  
Finite Element in Time, To appear in  
10th Anniversary of Vertica, Special  
Issue, 1986.
  
14. Pitt, D.M and Peters, D.A.,        Theoretical Prediction of Dynamic Inflow  
Derivatives" Vertica, Vol. 5, No. 1,  
1981, pp. 21-34.
  
15. Panda B. and Chopra I.            Flap-lag-torsion Stability in Forward  
Flight, Journal of the American  
Helicopter Society, Vol. 30, No. 4, Oct.  
1985, pp. 30-39.

TABLE 1 - CCR Rotor Characteristics in Analysis

Rotor radius R	28.5 ft.
Tip speed $\Omega R$	500 ft/sec.
Airfoil thickness ratio, t/c	0.17
Slot height-to-chord ratio, h/c	0.002
Reference lift curve slope, a	6.7
Vertical cg offset from hub, h	0.2R
Duct speed of sound $a_{duct}$	1274 ft/sec
Duct friction loss coefficient, $\eta_{duct}$	0.15
Centrifugal pumping efficiency, $\eta_{pump}$	0.57
Root radius-to-rotor radius ratio, $(r/R)_{root}$	0.13

Table 2 Structural properties of elements for the circulation control bearingless blade

Element	Length $\lambda/R$	Flapwise $EI_y/m_o\Omega^2R^4$	Chordwise $EI_z/m_o\Omega^2R^4$	Torsion $GJ/m_o\Omega^2R^4$	Mass $m/m_o$	Torsion inertia $K_m^2/R^2$	
1	0.2	0.0186	0.2303	0.0297	0.7067	0.000739	Blade
2	0.2	0.0372	0.3938	0.0557	1.0	0.000832	Blade
3	0.2	0.0929	0.7133	0.0929	1.624	0.001068	Blade
4	0.2	0.1858	0.2303	0.00297	1.383	0.000099	Flexbeam
5	0.2	0.5573	0.6687	0.00297	1.556	0.000279	Flexbeam
6	0.13	0.0817	0.5201	0.1560	1.398	0.001397	Torque tube
7	0.13	0.1486	0.3901	0.2823	1.549	0.001366	Torque tube

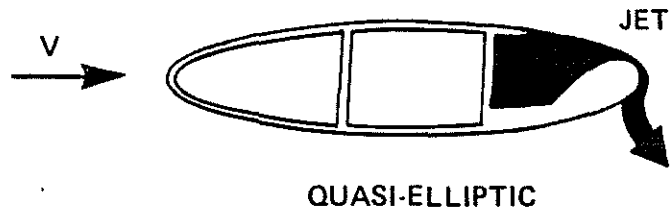


Figure 1. - Circulation control airfoil.

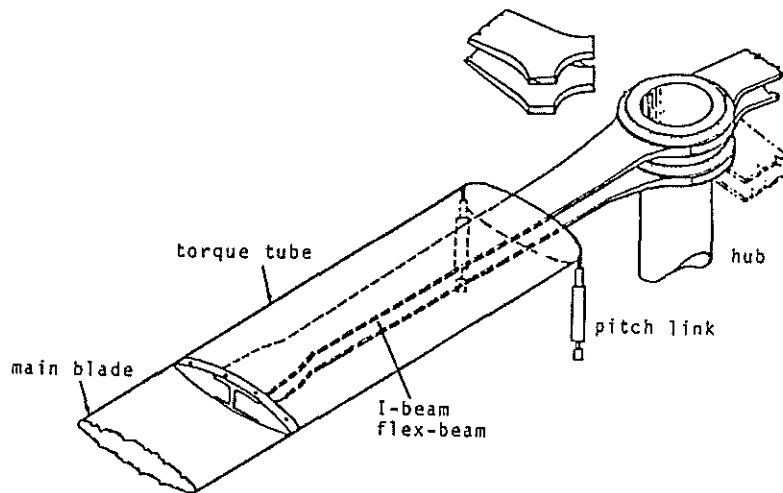
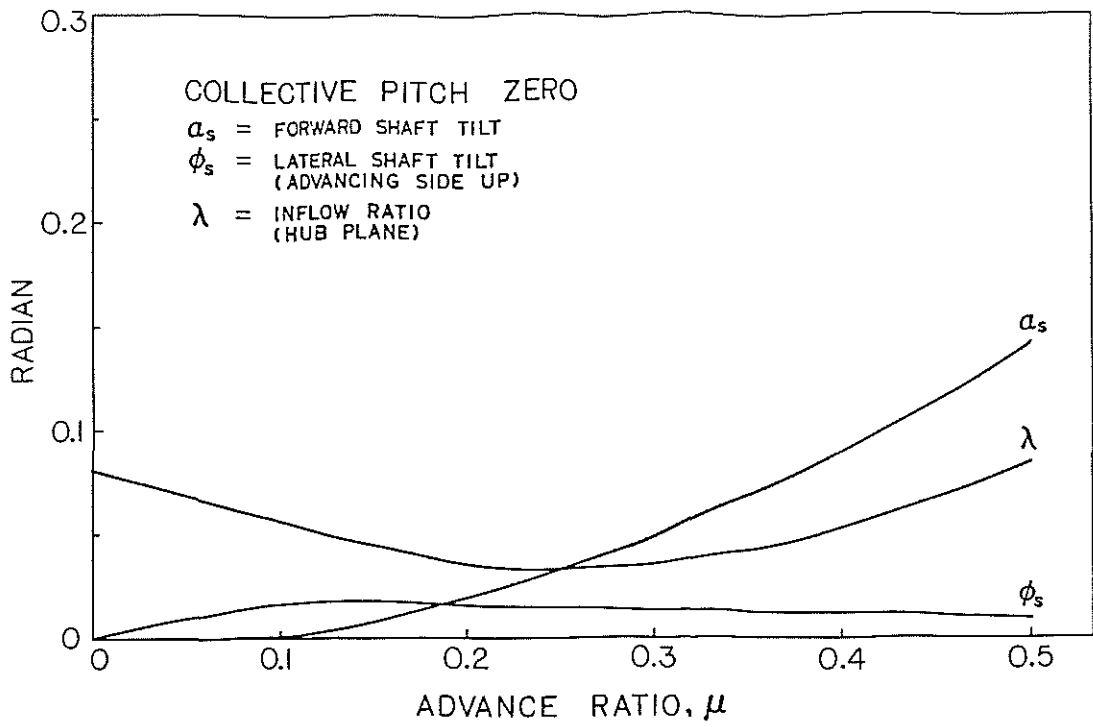
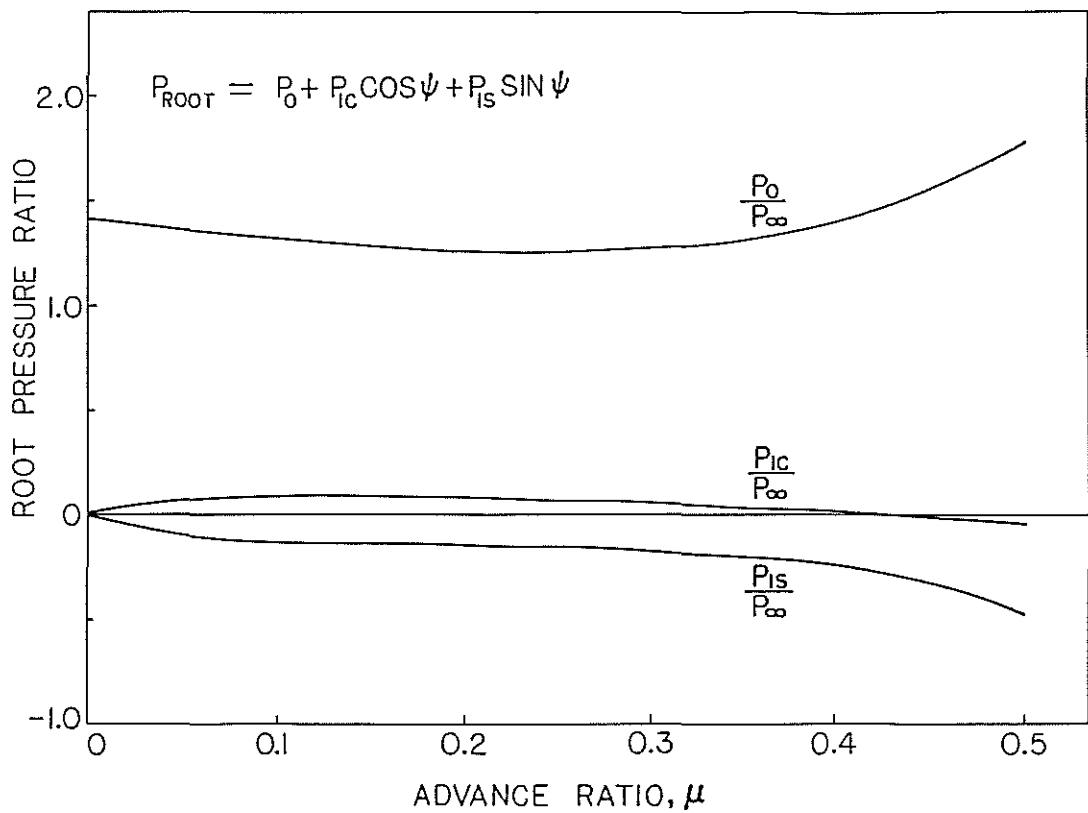


Figure 2. - Bearingless rotor blade.



(a) Rotor altitude and mean inflow.



(b) Blowing pressure requirements for trim.

Figure 3. - Vehicle propulsive trim solutions for a collective pitch of zero degree.

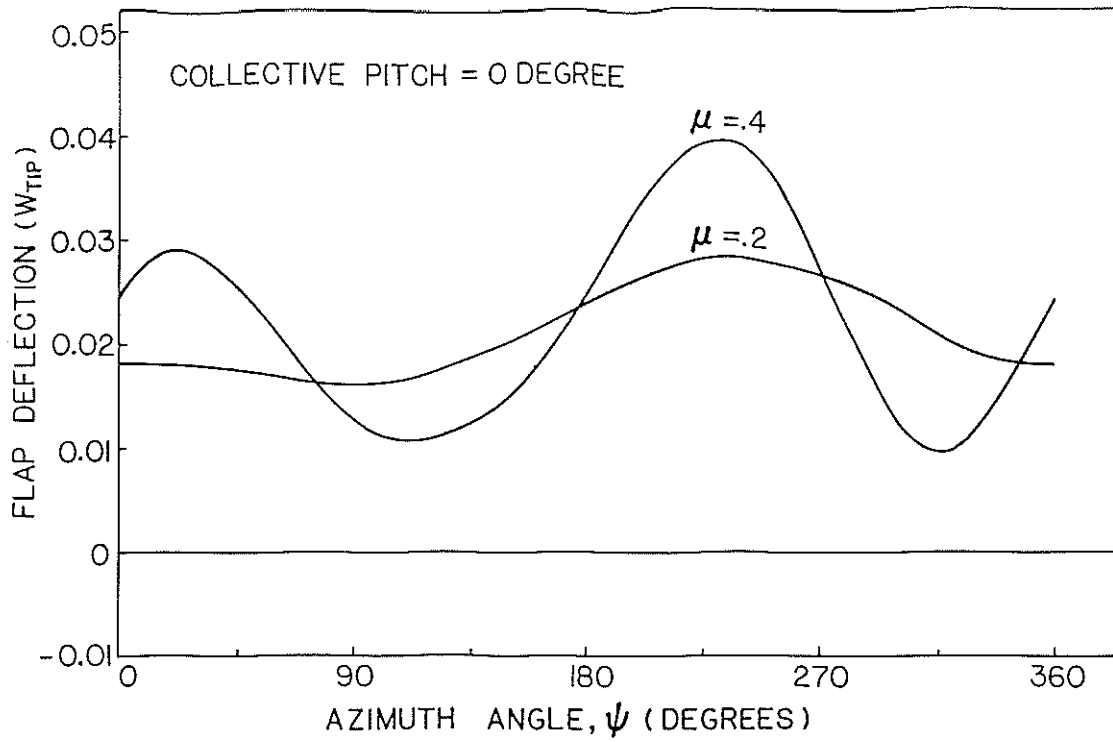


Figure 4. - Blade flap deflections( $W_{tip}$ ).

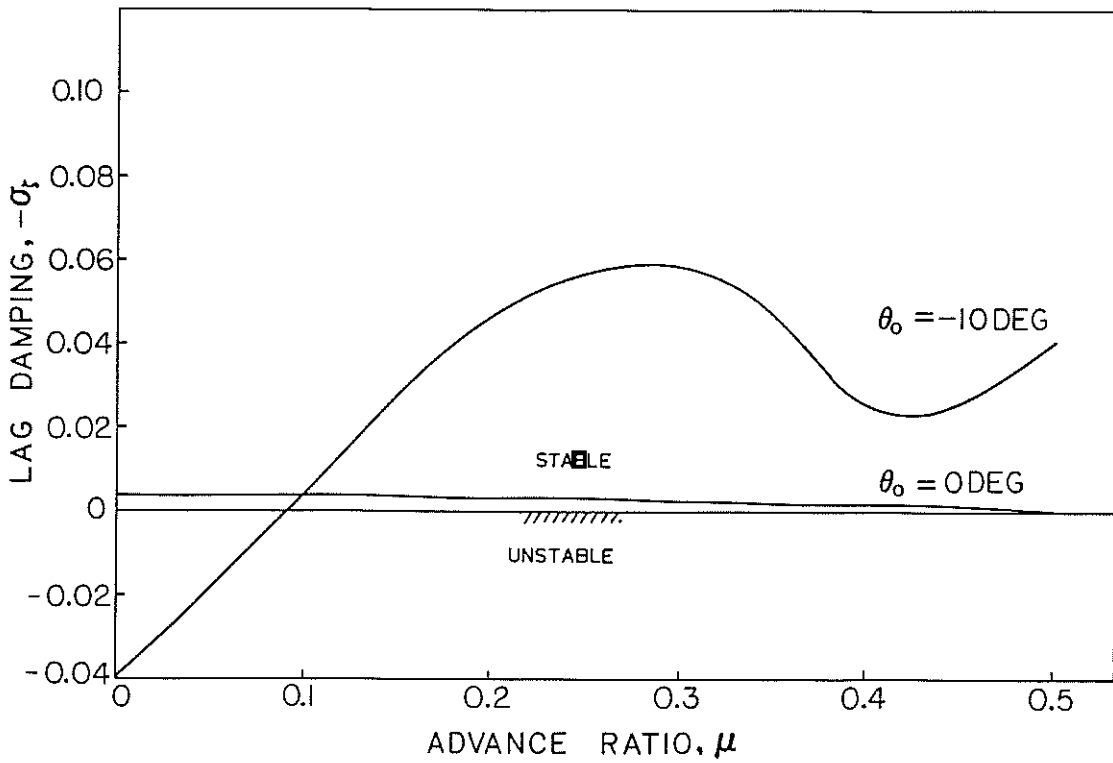


Figure 5. - Effect of collective pitch on low frequency cyclic lag mode.

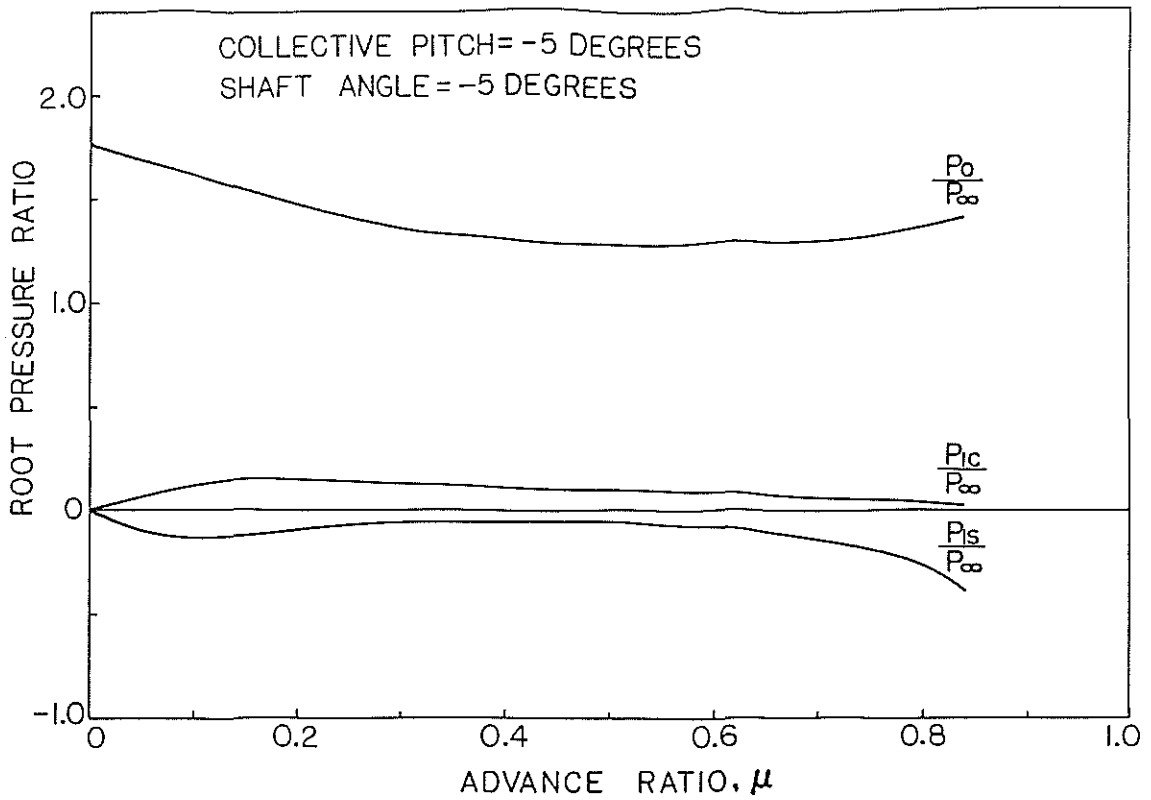


Figure 6. - Blade root blowing pressure requirements for the auxiliary power trim solution.

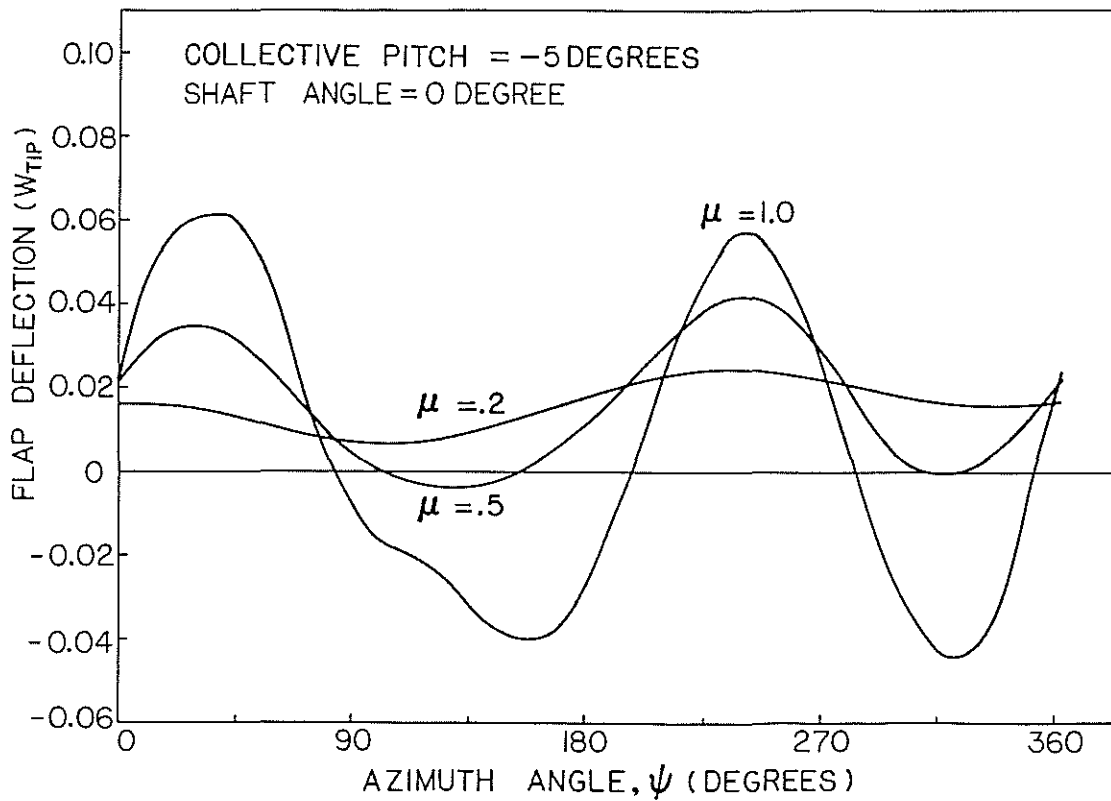


Figure 7. - Blade flap deflections ( $W_{tip}$ ).

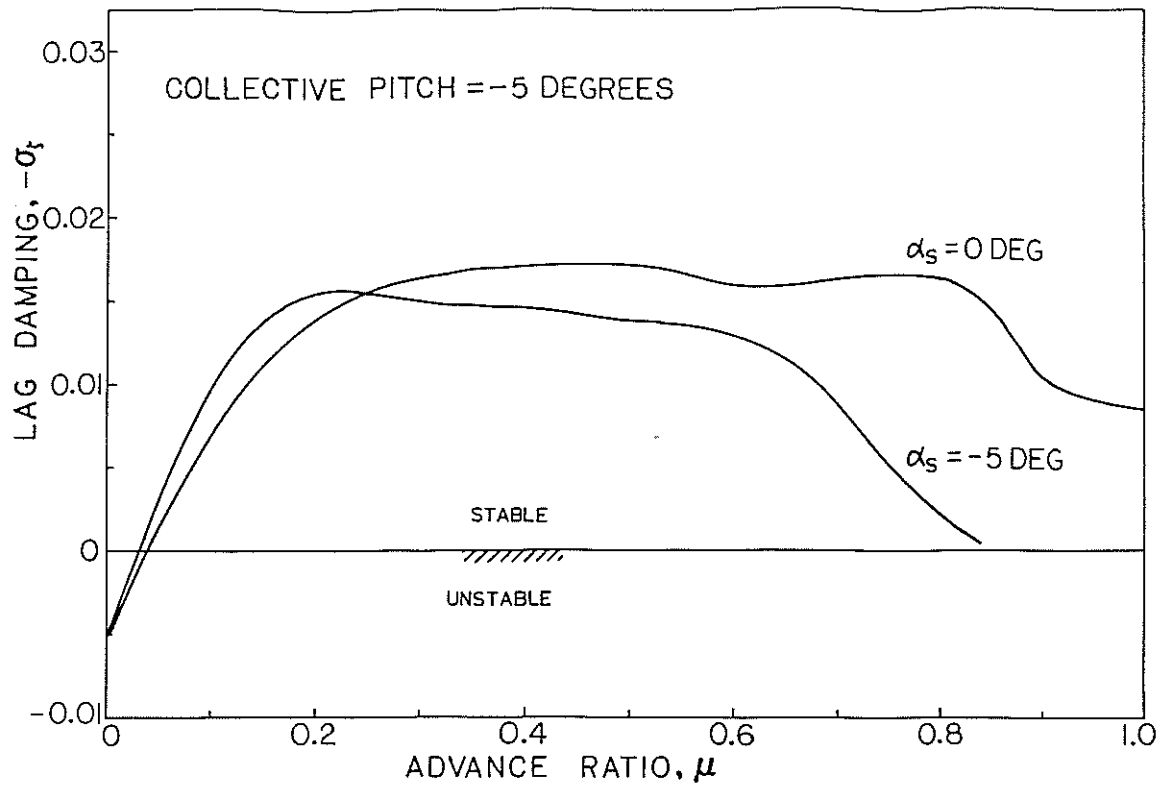


Figure 8. - Effect of shaft tilt on low frequency cyclic lag mode.